Pushing seismic resolution to the limit with FWI imaging

Zhiyuan Wei[1], Jiawei Mei[1], Zedong Wu[1], Zhigang Zhang[1], Rongxin Huang[1], and Ping Wang[1]

https://doi.org/10.1190/tle42010024.1

Abstract

Although the resolution of a seismic image is ultimately bound by the spatial and temporal sampling of the acquired seismic data, the seismic images obtained through conventional imaging methods normally fall very short of this limit. Conventional seismic imaging methods take a piecemeal approach to imaging problems with many steps designed in preprocessing, velocity model building, migration, and postprocessing to solve one or a few specific issues at each step. The inefficacies of each step and the disconnects between them lead to various issues such as velocity errors, residual noise and multiples, illumination holes, and migration swings that prevent conventional imaging methods from obtaining a high-resolution image with good signal-to-noise (S/N) and well-focused details. In contrast, full-waveform inversion (FWI) imaging models and uses the full-wavefield data including primaries and multiples and reflection and transmission waves to iteratively invert for the velocity and reflectivity in one go. It is a systemic approach to address imaging issues. FWI imaging has proven to be a superior method over conventional imaging methods because it provides seismic images with greatly improved illumination, S/N, focusing, and resolution. We demonstrate with a towed-streamer data set and an ocean-bottom-node (OBN) data set that FWI imaging with a frequency close to the temporal resolution limit of seismic data (100 Hz or higher) can provide seismic images with unprecedented resolution from the acquired seismic data. This has been impossible to achieve with conventional imaging methods. Moreover, incorporating more accurate physics into FWI imaging (e.g., upgrading the modeling engine from acoustic to elastic) can further improve the seismic resolution substantially. Elastic FWI imaging can further reduce the mismatch between modeled and recorded data, especially around bodies of large impedance contrast such as salt. It appreciably improves the S/N and resolution of the inverted images. We show with an OBN data set in the Gulf of Mexico that elastic FWI imaging further improves the resolution of salt models and subsalt images over its acoustic counterpart.

Introduction

High-resolution seismic images are important to energy exploration and production in many ways. They help in bypassing drilling hazards, identifying compartmentalized reservoirs, and placing offshore wind turbines. The resolution of a seismic image is fundamentally measured by two factors: the effective bandwidth and the number of octaves within the effective bandwidth. With noise that is inevitably present in seismic images of real data, the bandwidth is not simply a function of temporal and spatial samplings. Instead, only the frequency range where reasonable signal-to-noise (S/N) is present will contribute to the interpretable bandwidth. We refer to this as the effective bandwidth ($f_{max} - f_{min}$). Meanwhile, the number of octaves within the effective bandwidth, defined by $log_2\left(\frac{f_{max}}{f_{min}}\right)$, also matters. For the same effective bandwidth, a larger number of octaves will lead to fewer side lobes of the wavelets and higher resolution. Normally, the middle frequency bands have higher S/N than low- and high-wavenumber ends. Thus, the low- and high-wavenumber components generally dictate the resolution of a seismic image. The low-wavenumber resolution is mostly determined by factors such as the S/N of the low-frequency input data and velocity model accuracies. For the high-wavenumber part, in addition to the aforementioned factors, spatial and temporal samplings can become prominent limits. The goals of the conventional seismic imaging process are to improve the S/N of the input data (especially at the low- and high-frequency ends), derive an accurate velocity model that can properly map the energies from the time to depth domain, and eventually arrive at a well-focused and well-resolved image.

The conventional seismic imaging process takes a piecemeal approach to imaging problems with numerous steps designed in preprocessing, velocity model building (VMB), migration, and postprocessing to solve one or a few specific issues at each step. For example, to improve the low-frequency content in the data, deghosting (removing the source- and receiver-side ghosts) is performed to increase the low-frequency S/N of the input data and improve the low-wavenumber resolution of migration images (Wang et al., 2013). However, the efficacy of deghosting is often limited by the spatial sampling and S/N of the input data. Another case in point is multiple attenuation, which is time consuming. It is also very difficult to completely remove multiples without damaging primary signals. More importantly, valuable information contained in the multiple energy that is essential for vertical and lateral resolution is discarded. This is because most conventional imaging methods cannot properly handle multiple energy. Migration of multiples (Yang et al., 2013) has been proposed to use the reflection multiples as input to infill illumination holes of primary energy and improve the vertical and lateral resolution over primary migrations. However, migration of multiples generally suffers from crosstalk noise among primaries and different orders of multiples (Yang et al., 2013). Although least-squares migration of multiples (Wong et al., 2014) can mitigate crosstalk noise to some extent through an iterative least-squares data-fitting process, such approaches often require primary-multiple separation because the modeling engine can only simulate part of the energy in the recorded full-wavefield data. In addition, the migrations need to use a velocity model obtained by separate VMB approaches with different input data and objective functions. This is usually not optimal to collapse all of the multiple energy used in the least-squares migration of multiples. In short,

[1]CGG, Houston, Texas, USA. E-mail: zhiyuan.wei@cgg.com; jiawei.mei@cgg.com; zedong.wu@cgg.com; zhigang.zhang@cgg.com; rongxin.huang@cgg.com; ping.wang@cgg.com.

DOI:10.1190/tle42010024.1

the limits of individual steps and the disconnects between them make it difficult for conventional imaging processes to deliver a high-resolution image with well-focused details as implied by the maximum migration frequency (Wei et al., 2021a).

Maximizing seismic resolution with FWI imaging

Full-waveform inversion (FWI) imaging (Zhang et al., 2020; Huang et al., 2021; Wei et al., 2021a, 2021b) models and uses the full-wavefield data including primaries and multiples (ghost included) and reflection and transmission waves to iteratively invert for reflectivity and velocity in one go. It is a systemic approach to imaging problems and provides an elegant solution to mitigate most of the previously discussed limits imposed on conventional imaging approaches. Next, we will explain how FWI imaging can extract the full benefit of seismic data for optimal low- and high-wavenumber resolution with superior S/N and focusing.

FWI imaging (by running the inversion with many iterations at each frequency step) can extract low-wavenumber information as much as possible from the input data. Conversely, it is often difficult for conventional imaging methods to generate high S/N in the low-frequency end. For example, noise attenuation is a necessary step in conventional imaging approaches to improve the S/N of migration input data. However, noise attenuation at the low-frequency end is difficult because S/N is often very low, and denoise performed in local windows with small subsets of the wavefield cannot effectively separate the signal from heavy background noise. For these reasons, output from the approaches often still contains considerable residual low-frequency noise with compromised low-frequency signals. In contrast, FWI imaging can use input data with minimal preprocessing so low-frequency signals are properly retained. FWI imaging works on the entire wavefield recorded by all of the shots and receivers in a survey and can effectively utilize low-wavenumber information contained in large-angle data (e.g., diving waves) that cannot be used in conventional imaging approaches. It can accurately handle low-frequency ghost effects by directly simulating them in the wave propagation and can further improve the low-wavenumber resolution (Wei et al., 2021b).

As for higher wavenumbers, there are two factors that enable FWI imaging to provide increased vertical and lateral resolution. First, FWI models different orders of multiple energy. This offers more small-angle illumination in addition to primary energy and increases the vertical and lateral resolution of the images. Second, diving-wave energy, which is treated as noise in conventional imaging methods, can be properly utilized in FWI imaging (Wei et al., 2021b).

FWI imaging obtains velocity and reflectivity in the same inversion using the same cost function. Therefore, the velocity is automatically consistent with the image for optimal focusing of all of the energy. By iteratively updating velocity from low to high frequencies, FWI imaging provides a proper low- and high-wavenumber velocity that can focus the full-bandwidth and full-wavefield seismic data. With iterative least-squares fitting of the full-wavefield data from low to high frequencies, the migration artifacts, noise in input data, and illumination issues due to imperfect acquisitions are automatically minimized in FWI images (Zhang et al., 2020; Huang et al., 2021).

Despite all of the advantages of FWI imaging in providing superior low- and high-wavenumber seismic resolution, accurate physics in the modeling and inversion of FWI is still critical to avoid crosstalk noise among different wave modes that could appear in FWI images. For example, in salt environments, strong elastic effects around salt bodies with large impedance contrasts can lead to smearing of the salt boundary and the introduction of salt haloes. Although the salt halo has a relatively small impact on kinematics and migration images, it will have a more pronounced impact on the FWI image because it is a normal derivative of the velocity model. Specifically, for cases such as subsalt reflectors underneath a steeply dipping salt flank or subtle image details such as fault planes near salt boundaries, the image will be adversely affected by the salt halo. With more accurate physics, such as upgrading the modeling engine from acoustic to elastic, the modeled reflection and transmission energies at large impedance contrasts have amplitudes and phases that better match the recorded data. This effectively reduces data misfits and improves the salt convergence (Elebiju et al., 2022; Wu et al., 2022). As a result, the salt halo is significantly reduced in the elastic time-lag full-waveform inversion (E-TLFWI) velocity model, and the resulting FWI image has better-focused energy and higher S/N compared to its acoustic counterpart.

We have observed from previously published results that lower-frequency FWI imaging shows promising results, with improved S/N and better structural continuity over conventional imaging methods in various geologic settings such as subsalt and gas environments (Huang et al., 2021). It will be intriguing to compare FWI imaging at high frequencies reaching the temporal resolution limit (100 Hz and higher) to conventional Kirchhoff or reverse time migration (RTM) images by using different data types such as towed-streamer data and ocean-bottom-node (OBN) data. It will also be interesting to see how the resolution of FWI images can be further improved by considering the elastic effects in FWI.

Field data examples

Source-over-spread streamer data in the Barents Sea. We first examine the benefit of FWI imaging on a streamer data set by comparing it to conventional Kirchhoff, which is commonly considered to be the go-to product for high-resolution images. The data set comes from a source-over-spread narrow-azimuth towed-streamer survey (NATS) in the Greater Castberg area of the Barents Sea. The area features an iceberg-scoured highly rugose water bottom with shallow gas anomalies. This poses challenges for imaging the fault area in the deeper section.

In this survey, a group of five sources with a horizontal span of 300 m and firing every 37.5 m along the inline direction is placed at the center of 16 slant-towed streamers to acquire the near offsets for shallow imaging. Another front source is towed by the streamer vessel to provide long offsets up to 8.2 km for VMB (Vinje et al., 2017; Kerrison et al., 2021; Salaun et al., 2021; Wei et al., 2021a, 2021b). The cable spacing is 60 m between streamers, and the receiver interval along each cable is 12.5 m.

By using the acquired data right after deblending without any further processing, we ran TLFWI (Zhang et al., 2018) from the lowest usable frequency of the data at 3 Hz up to the imaging

frequency at 100 Hz and compared the FWI images with the Kirchhoff results. Figures 1a–1d show depth slices at 600 m for the TLFWI models at 15, 25, 50, and 100 Hz. This gradually reveals more details in the velocity models as the frequency increases. Correspondingly, the resolution of the FWI images continues to improve when moving to higher frequencies (Figures 2a–2d). Figure 2a shows the Kirchhoff image migrated with the 15 Hz TLFWI model using the input data that went through a conventional processing flow including denoise, deghost, demultiple, and data regularization. As we can see, the image quality of the 100 Hz FWI image is much better than the 100 Hz Kirchhoff image, with more clearly defined fault planes and better-imaged small channels and other geologic details. These features are either less obvious or completely

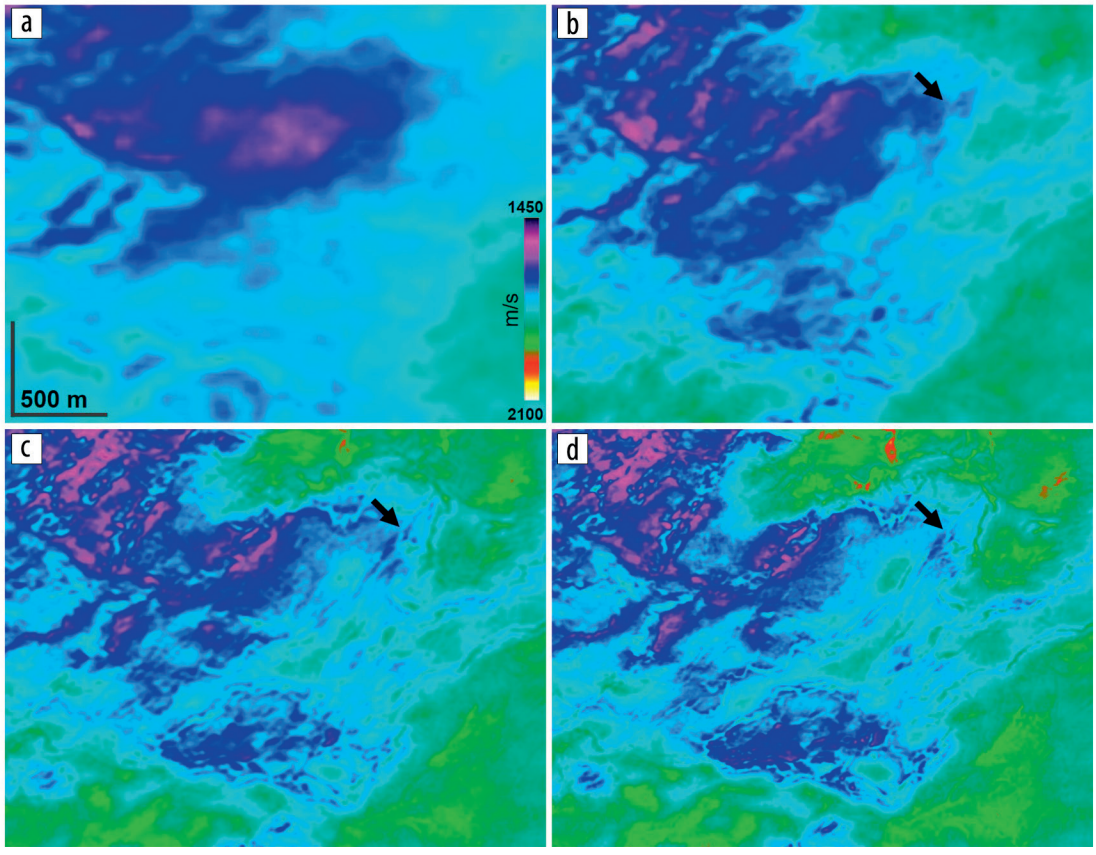

Figure 1. Depth slices at 600 m of a Barents Sea source-over-spread NATS data set. (a) 15 Hz TLFWI model. (b) 25 Hz TLFWI model. (c) 50 Hz TLFWI model. (d) 100 Hz TLFWI model. The high-frequency FWI models show better details.

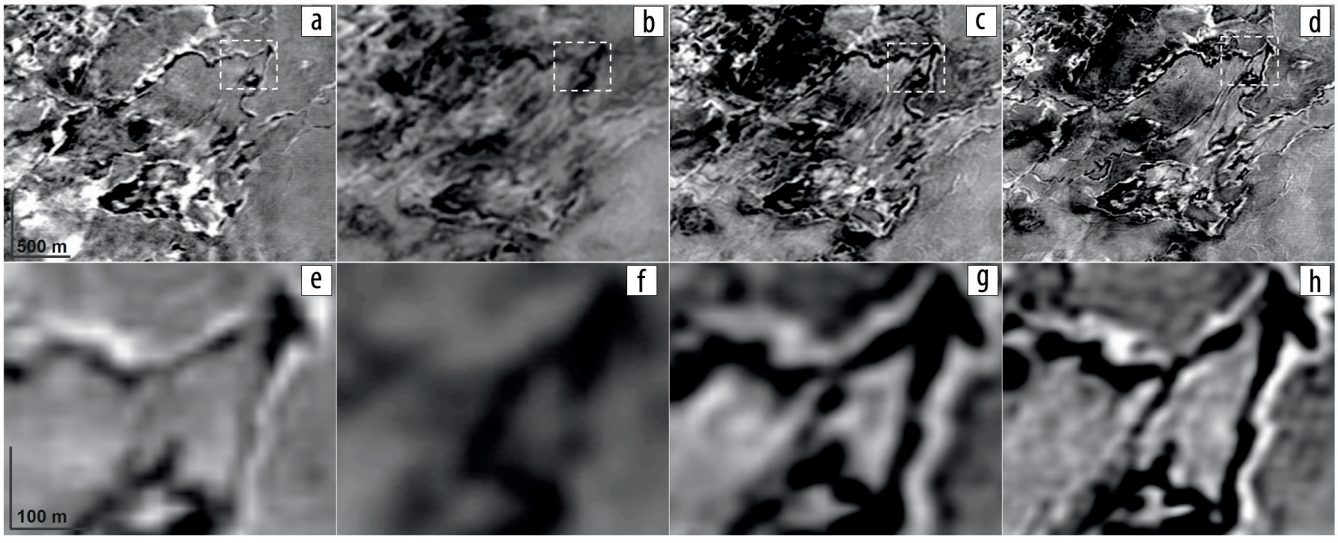

Figure 2. Depth slices at 600 m of a Barents Sea source-over-spread NATS data set. (a) 100 Hz Kirchhoff image with the 15 Hz TLFWI model in Figure 1a. (b) 25 Hz FWI image. (c) 50 Hz FWI image. (d) 100 Hz FWI image. (e)–(h) The zoomed-in sections of the white rectangles in (a)–(d), respectively. The high-frequency FWI images show better structure details such as faults and channels.

DOI:10.1190/tle42010024.1

missing in the counterpart Kirchhoff image. We can also observe better-imaged geologic details from the coherence attribute extracted from the seismic images (Chopra and Marfurt, 2018). The coherence attribute from the FWI image (Figures 3b and 3d) shows more clearly defined small-scale features of better S/N than the coherence attribute from Kirchhoff (Figures 3a and 3c).

The improved vertical and lateral resolution of the TLFWI models and the corresponding FWI images can also be observed from the section views (Figures 4 and 5). Similar to the observations from the depth slices, details of the velocity models from 25, 50, and 100 Hz gradually increase, and the resolution of the FWI images progressively improves. Structures such as faults are more precisely defined in higher-frequency FWI images, and the 100 Hz FWI image shows a much better resolution than the 100 Hz Kirchhoff image. It is also worth noting that FWI images have a broader bandwidth than Kirchhoff images, based on the band-limited images shown in Figure 6. From the images in different frequency bands (0–4, 4–8, 8–16, and 64–100 Hz), we notice that the S/N of the FWI images is better than the Kirchhoff images. Particularly, the FWI image at the very low-frequency end (Figure 6e) has less swing noise and shows some coherent events that consistently appear in higher-frequency images (Figures 6f and 6g). Such events are missing in the Kirchhoff image (Figure 6a). We think this is mainly due to two factors: (1) FWI can better compensate for the ghost effect through modeling and improve the low-wavenumber S/N and (2) FWI as an iterative data-fitting process takes many iterations to optimize low wavenumbers in the velocity model by matching modeled data with the recorded full-wavefield data. At the high-frequency end, fault energy is better focused in the FWI image (Figure 6h), while the Kirchhoff image (Figure 6d) suffers from contamination of migration swings that overshadow the subtle faults. Based on observations from the low- and high-frequency images, the previously observed superior resolution of FWI images over Kirchhoff is likely attributed to improved S/N at the low- and high-frequency ends. Thus, the effective bandwidth is broadened and the number of octaves is increased.

While reservoir images in deeper sections are often of major interest, high-resolution shallow seismic images are also important for bypassing drilling hazards and optimizing well paths,

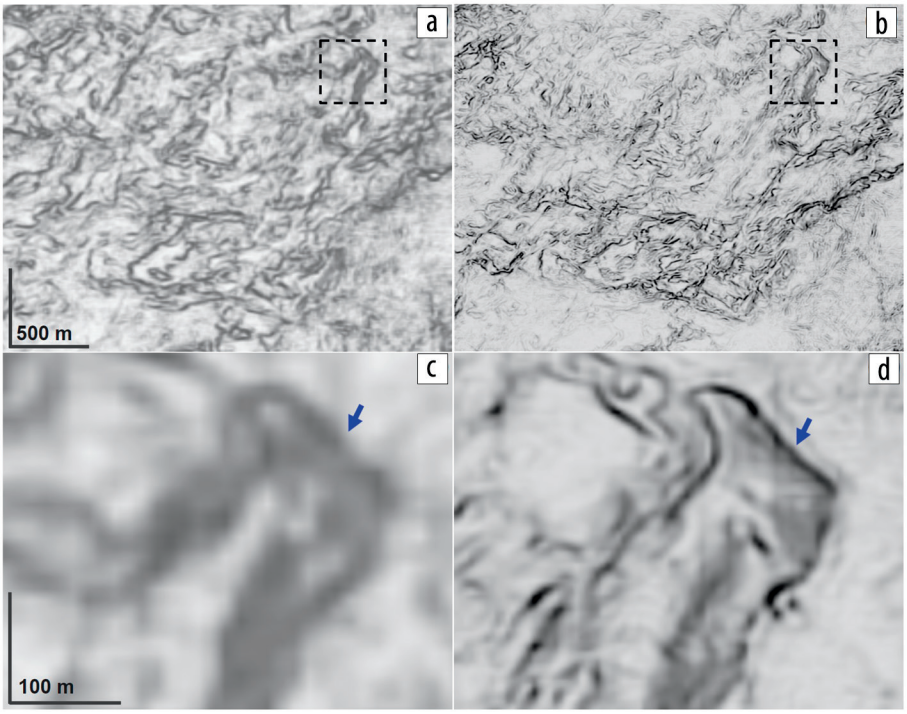

Figure 3. Depth view at 600 m of the coherence attribute extracted from (a) 100 Hz Kirchhoff image with the 15 Hz TLFWI model as shown in Figure 1a and (b) 100 Hz FWI image as shown in Figure 1h. (c) and (d) The zoomed-in displays of the areas marked by the black rectangles in (a) and (b), respectively. High-frequency FWI imaging provides superior resolution over Kirchhoff images.

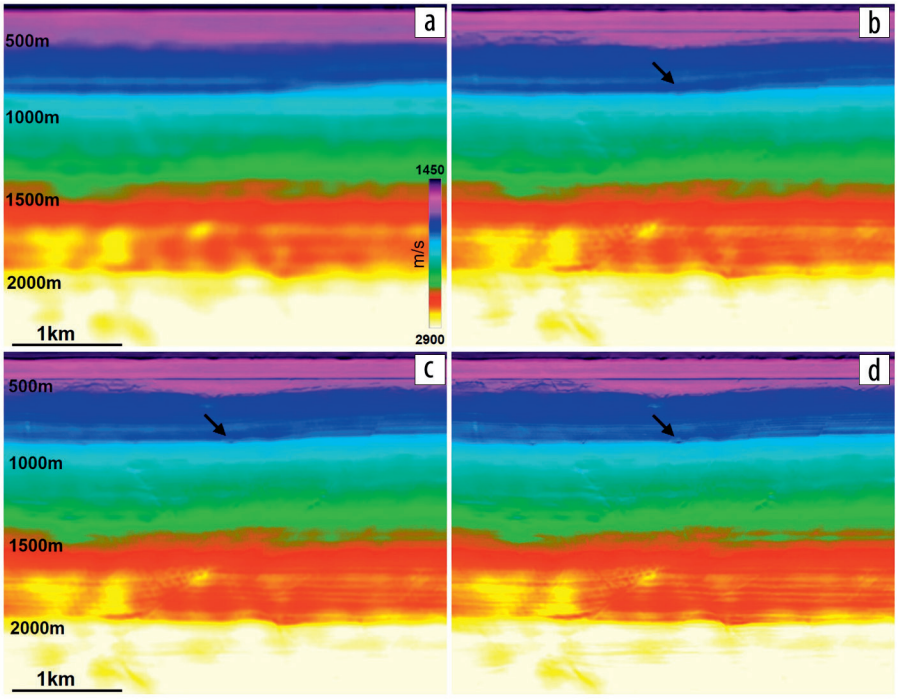

Figure 4. Section views of a Barents Sea source-over-spread NATS data set. (a) 15 Hz TLFWI model. (b) 25 Hz TLFWI model. (c) 50 Hz TLFWI model. (d) 100 Hz TLFWI model. The details of the velocity gradually increase as frequency increases.

DOI:10.1190/tle42010024.1

among other endeavors. In addition to superior resolution at reservoir level, high-frequency FWI imaging can provide improved resolution in shallow sections. Figures 7a and 7d show the shallow section views of a Kirchhoff image and FWI image. The FWI image shows higher lateral resolution and better structure variations (indicated by the orange arrow) than the Kirchhoff image (indicated by the red arrow). From the depth views (Figures 7b and 7d), small features such as iceberg scours are more precisely captured in the FWI image. Additionally, the acquisition footprints are less obvious in the FWI image than in the Kirchhoff, although data regularization/interpolation has been applied to the input data for the Kirchhoff image. Similarly, the coherency attributes (Figures 7c and 7f) also demonstrate that the FWI image shows higher S/N, better-defined small-scale shallow features, and higher resolution than the Kirchhoff image.

Shallow-water dense OBN data set. The benefits of FWI imaging in pushing the limits of image resolution can be more clearly demonstrated in a shallow-water dense OBN data set (Wei et al., 2021b). This OBN survey was designed to image the shallow hazard around existing platforms, and the data were acquired with denser

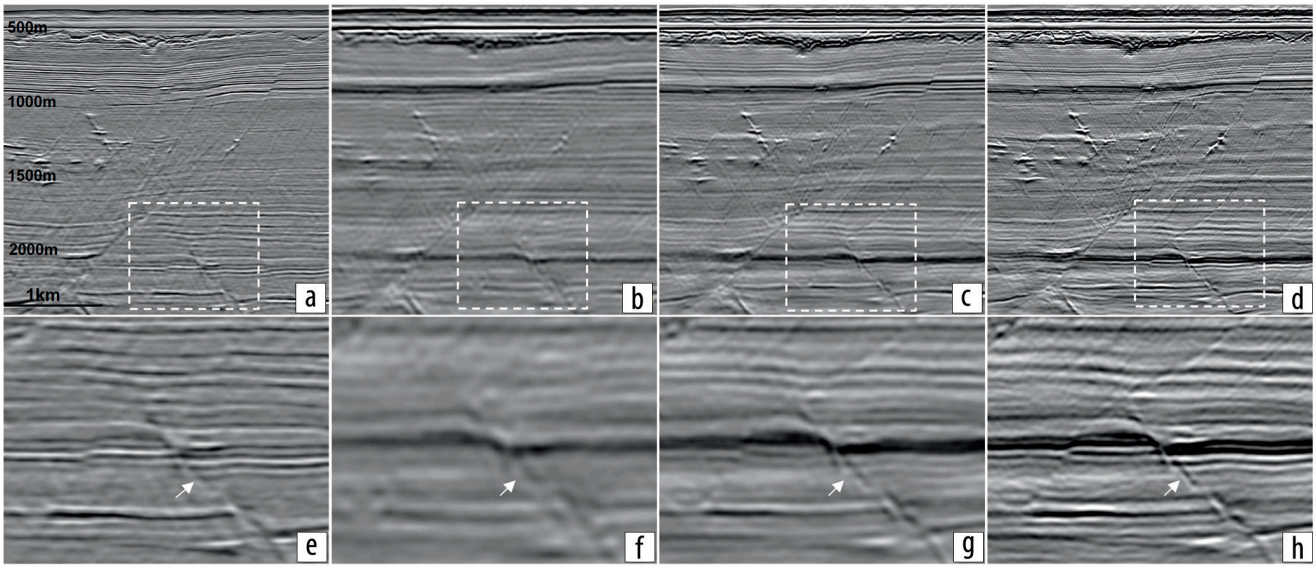

Figure 5. Section view of a source-over-spread NATS data set in the Barents Sea. (a) 100 Hz Kirchhoff image with the 15 Hz TLFWI model. (b) 25 Hz FWI image. (c) 50 Hz FWI image. (d) 100 Hz FWI image. (e)–(h) The zoomed-in displays of the white dashed rectangles in (a)–(d), respectively. High-frequency FWI imaging provides well-focused geologic details (Wei et al., 2021a).

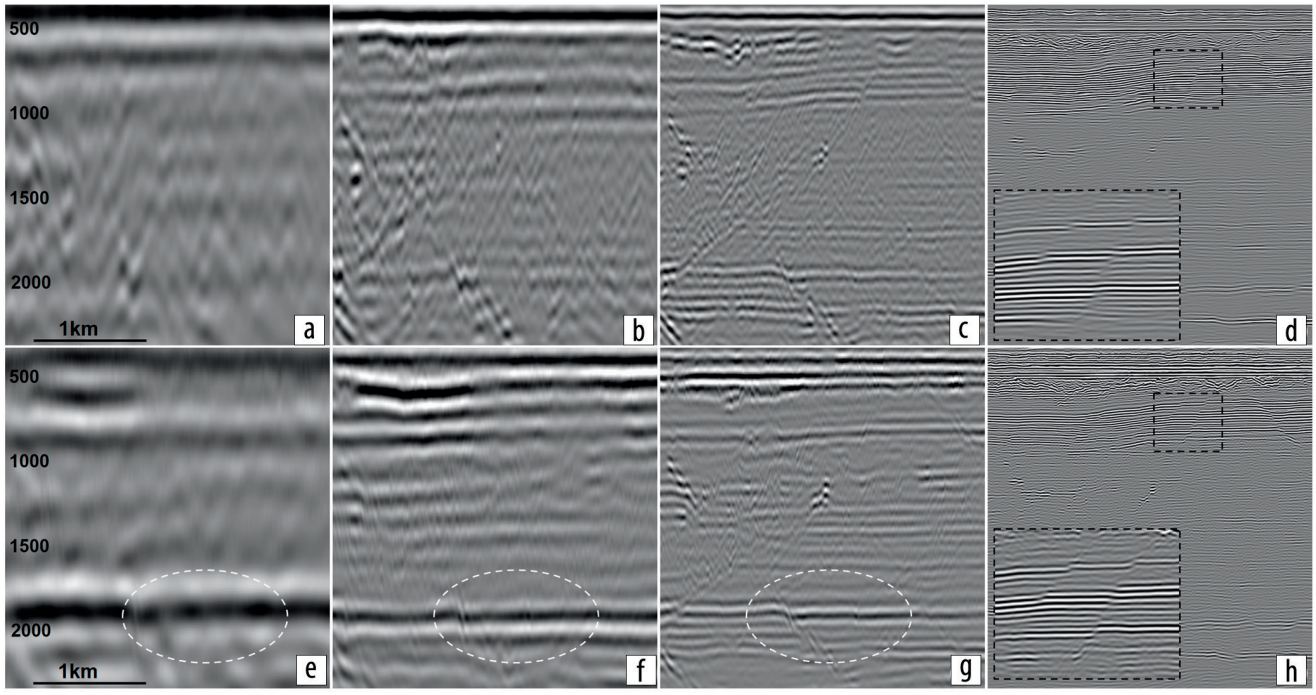

Figure 6. Section view of band-limited stack images from a source-over-spread NATS data set in the Barents Sea. (a) 0–4 Hz Kirchhoff stack. (b) 4–8 Hz Kirchhoff stack. (c) 8–16 Hz Kirchhoff stack. (d) 64–100 Hz Kirchhoff stack. (e) 0–4 Hz FWI image. (f) 4–8 Hz FWI image. (g) 8–16 Hz FWI image. (f) 64–100 Hz FWI image. Better S/N is observed in the FWI images at low, mid, and high frequencies (Wei et al., 2021a, 2021b).

node and shot samplings than normal OBN surveys. Due to platform obstacles, the nodes were deployed underneath the platforms with a nominal spacing of 50 × 50 m. The sources were shot around the platforms with a nominal spacing of 6.25 × 12.5 m.

Using the same workflow as in previous examples, we performed TLFWI updates using raw field data from the lowest usable frequency from 1.5 to 150 Hz to obtain the high-frequency velocity model and to derive the high-resolution FWI image (Figures 8a and 8b). The results are compared to the 150 Hz RTM image migrated with preprocessed downgoing wavefield data using a legacy model (Figure 8c). Overall, the 150 Hz FWI image provides better structure information, such as more continuous events with less undulations, better-defined fault planes, shallow diffractors, and deep gas pockets. The FWI image also extends the image area around the node coverage to a larger area approaching the boundary of the shot carpet and helps the imaging of a fault (white arrow in Figure 8b). We believe that this extra structural information is provided by the additional illumination gained from the inclusion of multiples and diving waves, which can be effectively utilized by inversion-based FWI imaging but are removed in the primary reflection data for RTM. Additionally, the RTM image seems to lack low-wavenumber content compared to the FWI image. Thus, the image of gas pockets in the deeper section can be better seen in the FWI image.

Besides the better-resolved shallow geologic features, FWI imaging can also provide extraordinary image resolution to reveal some small man-made features such as platform legs and subsea pipelines. A section view across the water column is shown in Figure 9a where we can see the legs of two platforms as highlighted by the blue arrows. A depth slice through the water bottom is shown in Figure 9b that clearly reveals the subsea pipelines as indicated by the blue arrows. Such small man-made features were

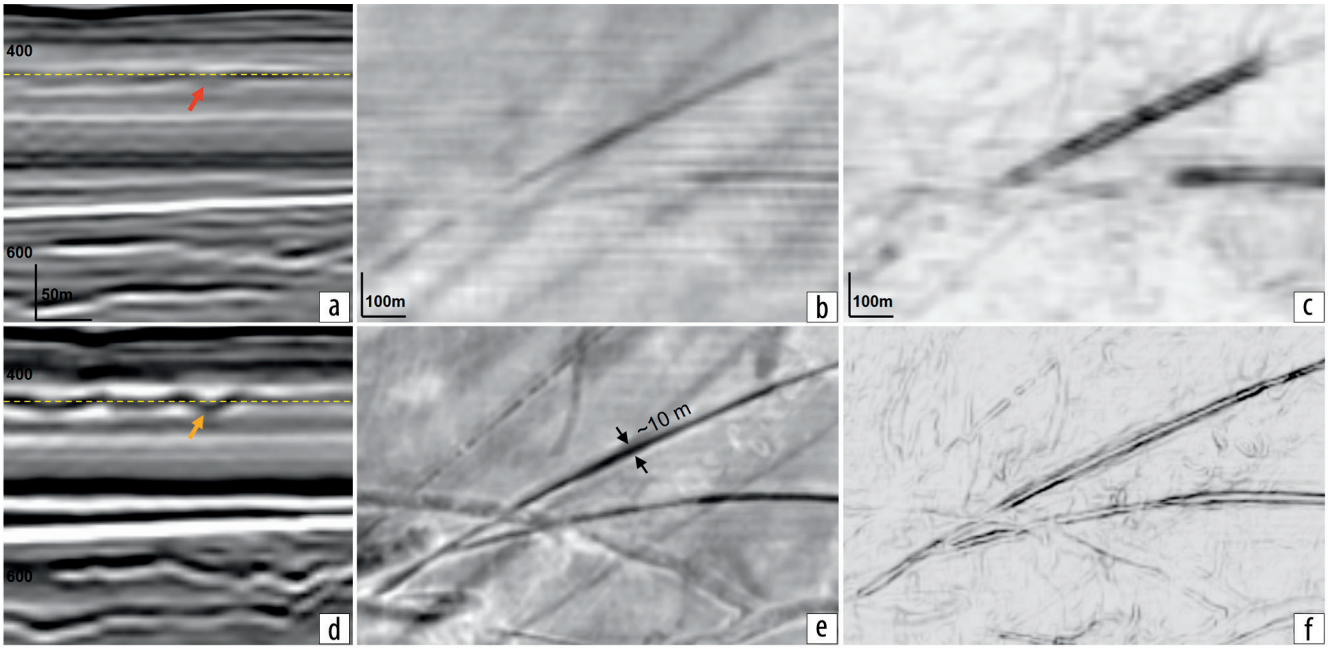

Figure 7. Shallow image of a source-over-spread NATS data set in the Barents Sea. (a) Shallow section view of the Kirchhoff stack. (b) Depth view at 450 m of the Kirchhoff stack. (c) Coherency attribute at a depth of 450 m extracted from the Kirchhoff stack. (d) Shallow section view of the FWI image. (e) Depth view at 450 m of the FWI image. (c) Coherency attribute at a depth of 450 m extracted from the FWI image. The yellow dashed line in (a) and (d) indicates the depth level of the depth view. FWI imaging shows better shallow image details.

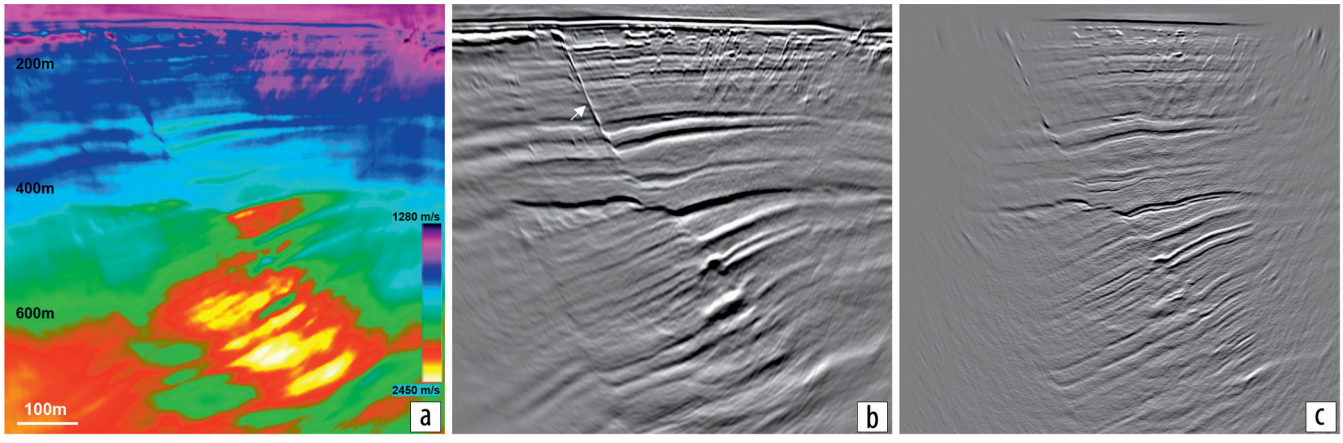

Figure 8. Section view of a shallow-water dense OBN data set. (a) 150 Hz TLFWI model. (b) 150 Hz FWI image. (c) 150 Hz RTM image. The FWI image better reveals faults, diffractors, and gas pockets (Wei et al., 2021b).

DOI:10.1190/tle42010024.1

rarely imaged previously with seismic data using conventional imaging methods. Similarly, the imaging of these small features is mostly attributed to the much-improved lateral illumination from diving waves and multiples. This significantly improves the lateral resolution of the FWI model and the FWI image.

With a streamer and an OBN data example, we demonstrated that FWI imaging can provide superior seismic resolution that is impossible to achieve with other imaging methods. It is worth mentioning that the previous examples are in sediment environments without strong impedance contrast bodies, and missing elasticity in acoustic FWI imaging has a negligible impact on the image. In geologic settings with strong impedance contrasts such as salt, elastic effects can smear the salt boundary and result in salt haloes that could deteriorate reservoir images very close to salt (such as reflectors below a steeply dipping salt flank and image details around a salt boundary).

Elastic FWI imaging in Atlantis OBN. Next, we examine the impact of elastic effects on FWI images of Atlantis Field in the Gulf of Mexico. The field is one of the largest oil fields in the Gulf of Mexico. It is a compartmentalized anticline reservoir partially lying below a complex salt body that has many salt fingers. In 2014–2015, a wider-offset OBN survey was acquired with the aim of resolving the complex velocity in addition to its normal reservoir monitoring objective (Lewis et al., 2016). This OBN data set has good low frequencies down to 1.5 Hz and long offsets up to 30 km. The good input data are deemed as one of the key elements for the successful application of FWI for automated salt model building (Michell et al., 2017; Shen et al., 2017; Zhang

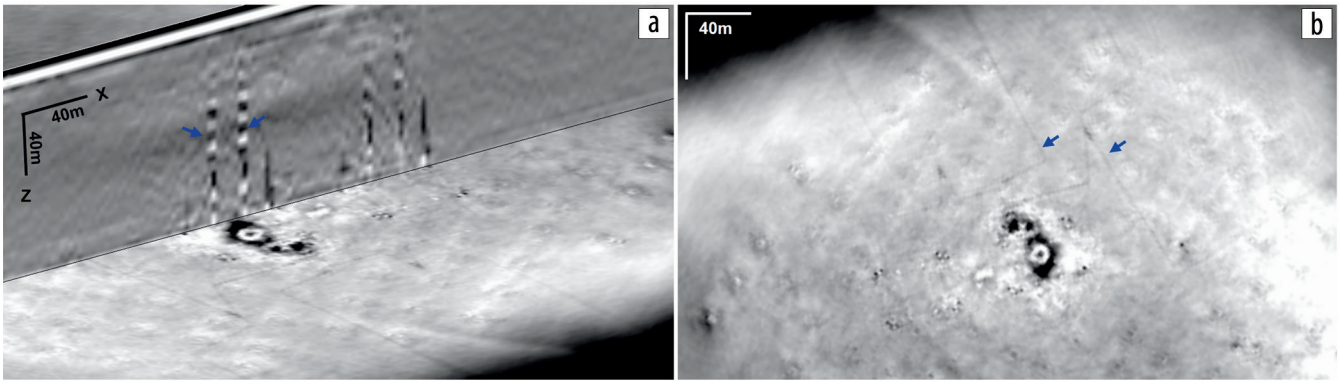

Figure 9. A 150 Hz FWI image from a shallow-water dense OBN data set. (a) Section view and (b) depth slice at 120 m. Man-made structures, such as platform legs and subsea pipelines, are resolved in the 150 Hz FWI image (Wei et al., 2021b).

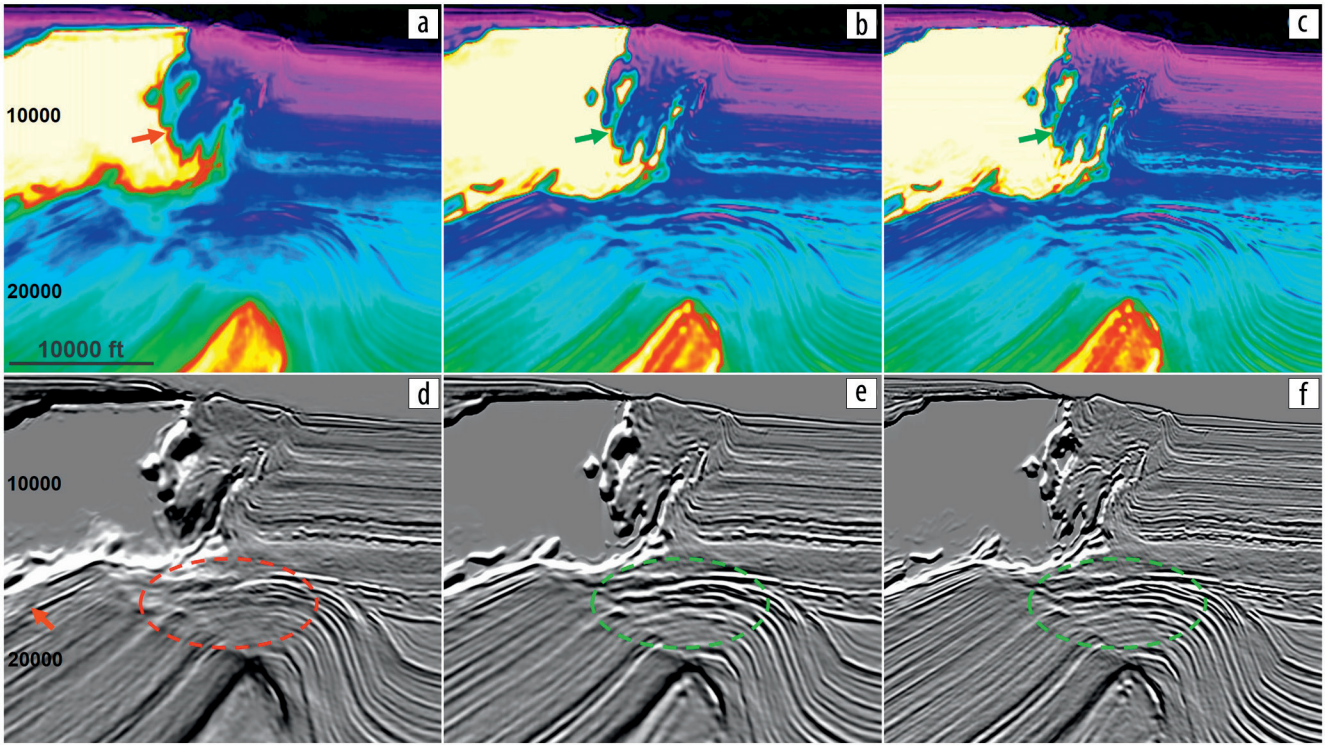

Figure 10. Section view of Atlantis OBN data. (a) 18 Hz A-TLFWI velocity model. (b) 18 Hz E-TLFWI velocity model. (c) 25 Hz E-TLFWI model. (d) 18 Hz A-TLFWI image. (e) 18 Hz E-TLFWI image (f) 25 Hz E-TLFWI image. The E-TLFWI models show sharpened salt boundaries and improved velocity details in sediments. The corresponding E-TLFWI images show better-defined salt boundaries and improved S/N and focusing.

DOI:10.1190/tle42010024.1

et al., 2018). With acoustic FWI using this data set, previous studies show that the velocity errors are less of a problem in this area than the illumination issues, and acoustic FWI imaging has shown greatly improved event continuity with higher S/N and higher resolution than conventional RTM in the subsalt low-illumination area (Zhang et al., 2020; Huang et al., 2021). However, the salt halo in the 18 Hz acoustic TLFWI (A-TLFWI) velocity model (Figure 10a) is apparent due to the missing elastic effects in acoustic FWI. When we run E-TLFWI to the same frequency of 18 Hz (Figure 10b), the salt halo in the E-TLFWI model (green arrows) is considerably reduced compared to the salt halo in the A-TLFWI velocity model (red arrows). This indicates that the elastic effects have significant impact on the sharpness of the inverted salt boundaries in addition to the inversion frequency. Besides sharper salt boundaries, the E-TLFWI model also shows clearer velocity contrasts and more details in sediment and subsalt areas than the A-TLFWI model. Running E-TLFWI to a higher frequency of 25 Hz further converges the velocity model, and the salt boundaries are sharpened. Moving to A-TLFWI and E-TLFWI images (Figures 10d and 10e), the missing elasticity in the A-TLFWI image leads to blurry salt boundaries, poorly defined image details such as fault planes, and some artifacts (red arrows). In contrast, the E-TLFWI image better reveals the reflectors around and below the salt with improved event continuity and better-defined faults. The higher-frequency E-TLFWI image of 25 Hz further sharpens the salt boundary and increases the image resolution. Similar observations can be made on depth views (Figures 11a and 11b), where the events from an open basin to the subsalt area (highlighted by green arrows) show higher S/N and more consistent amplitudes in the E-TLFWI image than in the A-TLFWI image. Moreover, the faults are also better defined in the E-TLFWI images. The 25 Hz E-TLFWI image further increased the image resolution over the 18 Hz E-TLFWI image (Figures 11b and 11c), and the improvements are more pronounced in the sediment area than in the subsalt low-illumination area.

Discussion

With the streamer and OBN data examples, we observed that FWI imaging shows obvious advantages in providing superior resolution over conventional imaging methods. To optimally collapse the energies of all frequencies into their correct positions for a high-resolution seismic image, a velocity model that is accurate from low to high wavenumbers is a factor of the upmost importance in FWI imaging. We previously observed that low- to mid-wavenumber components of a velocity model mostly determine the kinematics of migrations, while the high-wavenumber component does not visibly affect migration images. This is because migration algorithms typically assume a smooth velocity model and only handle single scattering energy. However, this does not hold true for inversion-based FWI imaging. The high-wavenumber component of the velocity model is equally essential for FWI imaging to explain the kinematics of low- and high-frequency energies, especially when the wavefield becomes complex around complicated geology and when multiple scattering energies need to be properly addressed.

However, the ability to obtain a velocity model that is accurate from low to high wavenumbers, and thus a high-resolution FWI image, is strongly limited by the available input data. A good input data set should provide sufficient constraints for the velocity model update from low to high wavenumbers. For the low-wavenumber part, this means input data with long-enough offsets, full-azimuth coverage, and good low-frequency S/N that allows FWI to correct for potentially large low-wavenumber velocity errors down to or beyond the target depth. For the high-wavenumber part, dense spatial sampling that can adequately sample the spatially fast-varying wavefield becomes important. If the spatial sampling is too sparse, it is difficult for FWI imaging to reconstruct the high-wavenumber velocity and image with high fidelity, even though additional illumination from multiples and diving waves is used. This can lead to images contaminated by footprints, swing noise, and other artifacts.

Good input data still need to pair with accurate physics in FWI, as well as accurate physical models, to achieve images of the highest possible resolution. We have observed that image resolution is improved when elastic effects are accounted for by elastic FWI in salt environments where the elasticity becomes dominant after the kinematics are reasonably resolved by acoustic FWI. In reality, the earth is much more complicated, and we need to consider earth attenuation in conjunction with elasticity

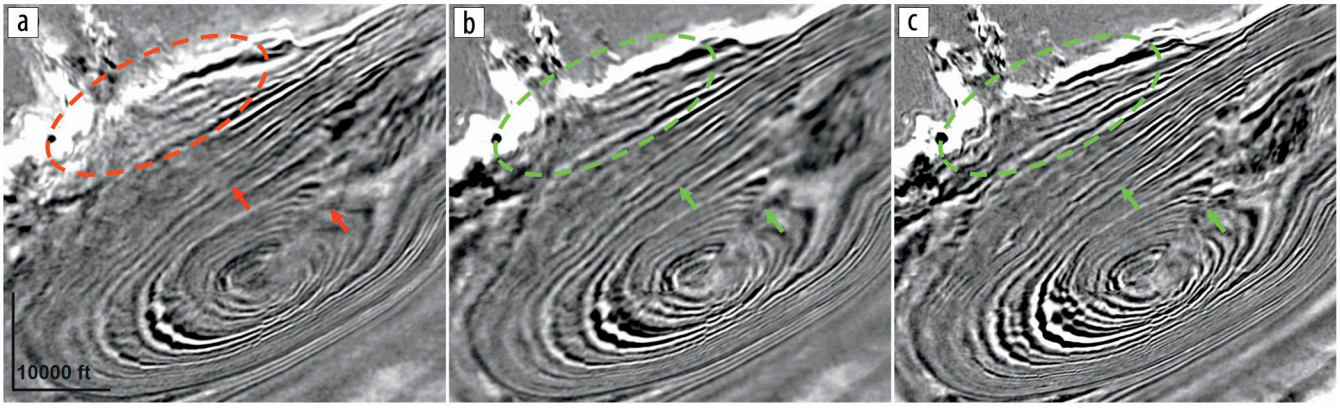

Figure 11. Depth view of FWI images from Atlantis OBN. (a) 18 Hz FWI image from A-TLFWI. (b) 18 Hz FWI image. (c) 25 Hz FWI image from E-TLFWI. The E-TLFWI images show improved continuity, higher S/N, and better-defined faults than the A-TLFWI counterpart.

(viscoelastic effect) and azimuthal anisotropy (orthorhombic effect). Accounting for these effects by having the complete physics in the FWI engine is certainly a good first step. However, we also need to have accurate physical models such as density, shear-wave velocity, attenuation Q, and tilted orthorhombic anisotropy (TOR) models to be able to accurately describe the wave propagation at the subsurface and precisely explain the recorded data. In this regard, data that provide good constraints to all of these physical models become essential. For example, single-azimuth data will not be sufficient for deriving reasonable TOR model parameters.

Finally, as we push FWI imaging toward higher frequencies and more accurate physics in the pursuit of unprecedented seismic resolution, the computational cost will inevitably increase exponentially. Significant effort is still needed to improve the efficiency of high-frequency FWI with the most-accurate physics and ensure that the cost of a high-resolution FWI image can be justified by its value.

Conclusions

We have demonstrated that FWI imaging can extract the full benefits of seismic data and yield unprecedented resolution, which has been impossible to achieve with conventional imaging approaches. FWI imaging can elegantly mitigate issues that come with conventional imaging methods such as velocity errors, migration artifacts, residual noise and multiples, and ghost effects. Additionally, the ability to handle diving waves and multiple energy in an iterative data-fitting manner enables FWI imaging to improve the vertical and horizontal resolution of images. We also demonstrated that with more accurate physics in FWI, elastic FWI imaging further improves the S/N and image resolution in areas around large impedance contrast bodies such as salt. As an innovative technology, FWI imaging makes it possible to push the seismic resolution to an unprecedented level and opens up many new opportunities that we can further explore with seismic data. TLE

Acknowledgments

We thank BP, Woodside Energy, TGS, and CGG for permission to publish this work.

Data and materials availability

Data associated with this research are confidential and cannot be released.

Corresponding author: zhiyuan.wei@cgg.com

References

Chopra, S., and K. J. Marfurt, 2018, Coherence attribute applications on seismic data in various guises — Part 1: Interpretation, **6**, no. 3, N512–N529, https://doi.org/10.1190/INT-2018-0006.1.

Elebiju, B., Q. Li, K. Hartman, F. Rollins, Y. Feng, K. Kaiser, W. Schinagl, C. Chen et al., 2022, One more stride forward in Thunder Horse subsalt imaging with elastic FWI: International Meeting for Applied Geoscience & Energy, SEG/AAPG, Expanded Abstracts, 947–951, https://doi.org/10.1190/image2022-3750987.1.

Huang, R., Z. Zhang, Z. Wu, Z. Wei, J. Mei, and P. Wang, 2021, Full-waveform inversion for full-wavefield imaging: Decades in the making: The Leading Edge, **40**, no. 5, 324–334, https://doi.org/10.1190/tle40050324.1.

Kerrison, H., P. Fallon, E. Kaszycka, K. Cichy, A. Ratcliffe, and N. Masmoudi, 2021, Impact of streamer acquisition geometry on FWI imaging: Presented at the 82nd Conference and Exhibition, EAGE.

Lewis, B., C. Brooks, M. Pfister, S. Michell, and G. Astvatsaturov, 2016, Efficient acquisition of deepwater node surveys: 86th Annual International Meeting, SEG, Expanded Abstracts, 92–96, https://doi.org/10.1190/segam2016-13867668.1.

Michell, S., X. Shen, A. Brenders, J. Dellinger, I. Ahmed, and K. Fu, 2017, Automatic velocity model building with complex salt: Can computers finally do an interpreter's job?: 87th Annual International Meeting, SEG, Expanded Abstracts, 5250–5254, https://doi.org/10.1190/segam2017-17778443.1.

Salaun, N., M. Reinier, I. Espin, and G. Gigou, 2021, FWI velocity and imaging: A case study in the Johan Castberg area: 82nd Conference and Exhibition, EAGE, Extended Abstracts, https://doi.org/10.3997/2214-4609.202112763.

Shen, X., I. Ahmed, A. Brenders, J. Dellinger, J. Etgen, and S. Michell, 2017, Salt model building at Atlantis with full-waveform inversion: 87th Annual International Meeting, SEG, Expanded Abstracts, 1507–1511, https://doi.org/10.1190/segam2017-17738630.1.

Vinje, V., J. E. Lie, V. Danielsen, P. E. Dhelie, R. Silliqi, C.-I. Nilsen, E. Hicks, and A. Camerer, 2017, Shooting over the seismic spread: First Break, **35**, no. 6, 97–104, https://doi.org/10.3997/1365-2397.35.6.89461.

Wang, P., S. Ray, C. Peng, Y. Li, and G. Poole, 2013, Premigration deghosting for marine streamer data using a bootstrap approach in tau-p domain: 83rd Annual International Meeting, SEG, Expanded Abstracts, 4221–4225, https://doi.org/10.1190/segam2013-0225.1.

Wei, Z., J. Mei, Z. Wu, Z. Zhang, R. Huang, and P. Wang, 2021a, FWI imaging: Revealing the unprecedented resolution of seismic data: First International Meeting for Applied Geoscience & Energy, SEG/AAPG, Expanded Abstracts, 682–686, https://doi.org/10.1190/segam2021-3583772.1.

Wei, Z., J. Mei, Z. Wu, Z. Zhang, R. Huang, and P. Wang, 2021b, Unlocking unprecedented seismic resolution with FWI imaging: Presented at the 82nd Conference and Exhibition, EAGE.

Wong, M., B. Biondi, and S. Ronen, 2014, Imaging with multiples using least-squares reverse time migration: The Leading Edge, **33**, no. 9, 970–976, https://doi.org/10.1190/tle33090970.1.

Wu, Z., Z. Wei, Z. Zhang, J. Mei, R. Huang, and P. Wang, 2022, Elastic FWI for large impedance contrasts: International Meeting for Applied Geoscience & Energy, SEG/AAPG, Expanded Abstracts, 3686–3690, https://doi.org/10.1190/image2022-w17-02.1.

Yang, Z., L. Chernis, W. Gou, S. Ji, Y. Li, and J. Hembd, 2013, Enhanced reverse time multiple migration and its applications: 83rd Annual International Meeting, SEG, Expanded Abstracts, 4121–4125, https://doi.org/10.1190/segam2013-0776.1.

Zhang, Z., J. Mei, F. Lin, R. Huang, and P. Wang, 2018, Correcting for salt misinterpretation with full-waveform inversion: 88th Annual International Meeting, SEG, Expanded Abstracts, 1143–1147, https://doi.org/10.1190/segam2018-2997711.1.

Zhang, Z., Z. Wu, Z. Wei, J. Mei, R. Huang, and P. Wang, 2020, FWI imaging: Full-wavefield imaging through full-waveform inversion: 90th Annual International Meeting, SEG, Expanded Abstracts, 656–660, https://doi.org/10.1190/segam2020-3427858.1.

DOI:10.1190/tle42010024.1